Tribology International 188 (2023) 108822

Contents lists available at ScienceDirect

Tribology International

journal homepage: www.elsevier.com/locate/triboint

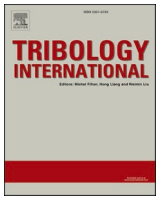

The combined effect of contact interface size and spin on lubricated traction in rolling-sliding point contacts

Mikel Iribecampos [a,*], Ibai Ulacia [a], Aitor Arana [a], Jon Larrañaga [a]

[a] Mondragon Unibertsitatea, Faculty of Engineering, Loramendi 4, Arrasate-Mondragon 20500, Spain

ARTICLE INFO

Keywords:
Traction
Elastohydrodynamic
Spinning
Sliding

ABSTRACT

Traction in lubricated rolling and sliding contacts plays an important role in the performance of several machine elements. Many of such elements are subject to spin motion, which can affect their performance. Recent studies have also highlighted the effects of the contact scale on the traction behaviour. Nevertheless, their combined effect was not investigated to date. The present study, therefore, analyses the effect of both on the traction in heavily-loaded lubricated contacts. To this end, a novel semi-analytical traction prediction model was developed considering spin motion. The results show that increasing the contact size and/or spinning speed leads to a reduction in traction coefficient and contact efficiency due to thermal effects. These conclusions have important practical applications designing machine elements.

1. Introduction

The traction coefficient under elastohydrodynamic lubrication (EHL) conditions plays an important role in the operation of several machine elements. Therefore, understanding the variables that impact traction is essential to accurately predict machine performance [1]. It is well established that the traction coefficient is influenced by many factors such as lubricant properties, rolling and sliding speeds, contact pressure, and temperature [2]. On the one hand, the rolling speed generates a fluid film that separates the two components in contact, which is determined by the lubricant properties at the inlet of the contact [3]. On the other hand, the sliding speed causes shearing of the lubricant, which is governed by the rheological properties of the lubricant in the Hertzian contact region. Contact pressure in this region also increases the viscosity of the lubricant [3]. Moreover, the shearing of the lubricant generates heat, leading to a rise in temperature in the contact interface [4]. This temperature increase can, in turn, decrease the viscosity of the lubricant and thus influence the traction behaviour of the contact point.

Many machine elements, such as angular contact ball bearings or toroidal continuously variable transmissions, are subject to spin motion which can significantly affect their performance [5–8]. Spin motion is defined as a circular sliding motion rotating around an axis normal to the contact interface. The point at which there is no sliding between the components in contact is known as the spin pole [9]. Spin induces local shear thinning in the lubricant and raises the contact temperature, which typically lowers the traction coefficient. This reduction in traction is particularly significant in low longitudinal sliding conditions [10]. Nevertheless, the additional sliding motion affects the contact conditions, resulting in increased power losses.

Recent studies have also highlighted the effects of the scale of the contact interface on the traction coefficient [11–14]. Experimental investigations have revealed that larger contact interfaces exhibit lower traction coefficient values under comparable working conditions (pressure, speed, and temperature) [12]. An isothermal analysis revealed differences in traction, however, these differences were lower than those obtained experimentally. Therefore, the authors attributed the reduction in traction to an increase in the contact temperature, which led to a subsequent reduction in the lubricant viscosity.

With the aim of predicting the traction coefficient, several lubricated traction prediction models have been proposed, which are mainly based on calculating the shear stresses of the lubricant film [15]. These models can be empirical, analytical or numerical. Empirical traction prediction models are based on traction measurements. Using a tribometer to measure many traction curves in multiple working conditions, these models determine the traction coefficient in each working condition via regression [16]. Numerical traction prediction models, on the other hand, consider the physical phenomena occurring inside the contact region. These have undergone significant improvements in recent years, in particular solving Reynold's flow equation together with load, energy, and elasticity balance equations. However, numerical methods can

* Corresponding author.
E-mail address: miribecampos@mondragon.edu (M. Iribecampos).

https://doi.org/10.1016/j.triboint.2023.108822
Received 2 June 2023; Received in revised form 13 July 2023; Accepted 21 July 2023
Available online 23 July 2023

be subject to some convergence issues and incur considerable computational costs [17–20]. Finally, simple and time efficient analytical traction prediction models have proven suitable for machine elements with multiple EHL working conditions. These models provide accurate traction results for engineering purposes [21–23]. However, for the sake of simplicity, this kind of models usually locate the spin pole position independently from real kinematic behaviour [24] giving rise to non-feasible solutions, rheological models do not account for high pressure viscosimetry [25] and the thermal calculation usually considers a constant, contact size independent, friction coefficient in the contact area [2].

Although the traction coefficient is influenced by both spin and contact size, their combined effect has not been investigated to date. The present study, therefore, analyses the effect of both parameters on the effective traction coefficient in heavily-loaded lubricated contacts. To this end, a semi-analytical traction prediction model has been developed, which takes into consideration the interrelation between local contact kinematics with spin, lubricant rheology, and contact temperature. The model is validated with published experimental traction measurements and then used to determine the traction coefficient for multiple spinning and contact sizes under comparable working conditions (lubricant, speed, pressure, and temperature). Finally, the contact efficiencies are also determined.

2. Traction in heavily-loaded lubricated contacts with spin

2.1. Generalized traction prediction model

Under high normal load conditions, the EHL pressure distribution on lubricated rolling point contacts resembles that of smooth dry contact and the film thickness shape within the contact region approximates to a constant value [26]. In such conditions, the EHL lubrication problem can be stated with the Ertel-Grubin approach [4]. This method is employed in the semi-analytical traction prediction model developed in this study.

Fig. 1 illustrates a lubricated elliptical contact interface in which the semi-minor axis is oriented to the rolling velocity component and aligned with the x-axis. The position of the spin pole is included to generalize the model to arbitrary contact conditions. Point O refers to the geometric origin of the contact ellipse while point P indicates the spin pole position.

Film thickness distribution inside the contact region is considered constant and equal to the central film thickness value h_c, and is calculated using the equation proposed by Chittenden et al. [27]. The pressure distribution $p(x,y)$, contact area A_H, and gap outside the interface $h(x,y)$, follow the Hertzian solution for general elliptical contacts, as presented by Moes [28]. For an arbitrary contact point Q inside the interface, local fluid traction $\tau(x,y)$ depends on local fluid pressure $p_f = p(x,y)$, film thickness h_c, and kinematic conditions.

Kinematic dispositions considering spin were defined by Loewenthal [9]. Spinning speed is usually quantified by the spin to roll ratio S_p, which is a dimensionless parameter as shown in Eq. 1.

$$S_p = \frac{\omega_s \cdot \sqrt{a \cdot b}}{u_e} \tag{1}$$

where ω_s is the spinning speed; a and b the semimajor and semiminor axis of the contact interface, respectively; and u_e the entrainment speed, defined as the mean rolling speed of the bodies in contact $u_e = (u_b + u_d)/2$.

Finally, from rigid body kinematics, and using vector composition, the spin pole position $\overline{PO}$ and local sliding speed distribution $v_s(x,y)$ can be computed. The former is determined from the overall sliding speed calculated at the centre of the contact O, while the latter also considers the distance from the centre of the contact to the evaluated point Q on the contact interface. Using standard notation shown in Fig. 1, the sliding speed v_s is defined as the difference between the rolling speeds of the bodies in contact, and thus its value in the centre of the interface is $v_s = u_b - u_d = \omega_{by} \cdot r_{bx} - \omega_d \cdot r_d$. Similarly, the spinning speed ω_s is the sum of the rotational speed in z-axis of both components in contact $\vec{\omega}_s = \vec{\omega}_{bz} + \vec{\omega}_d$. Matching the latter to the distance to the spin pole one yields Eq. 2 and finally the sliding speed distribution is obtained from Eq. 3. Thus, following Loewenthal [9] and contrary to other works in scientific

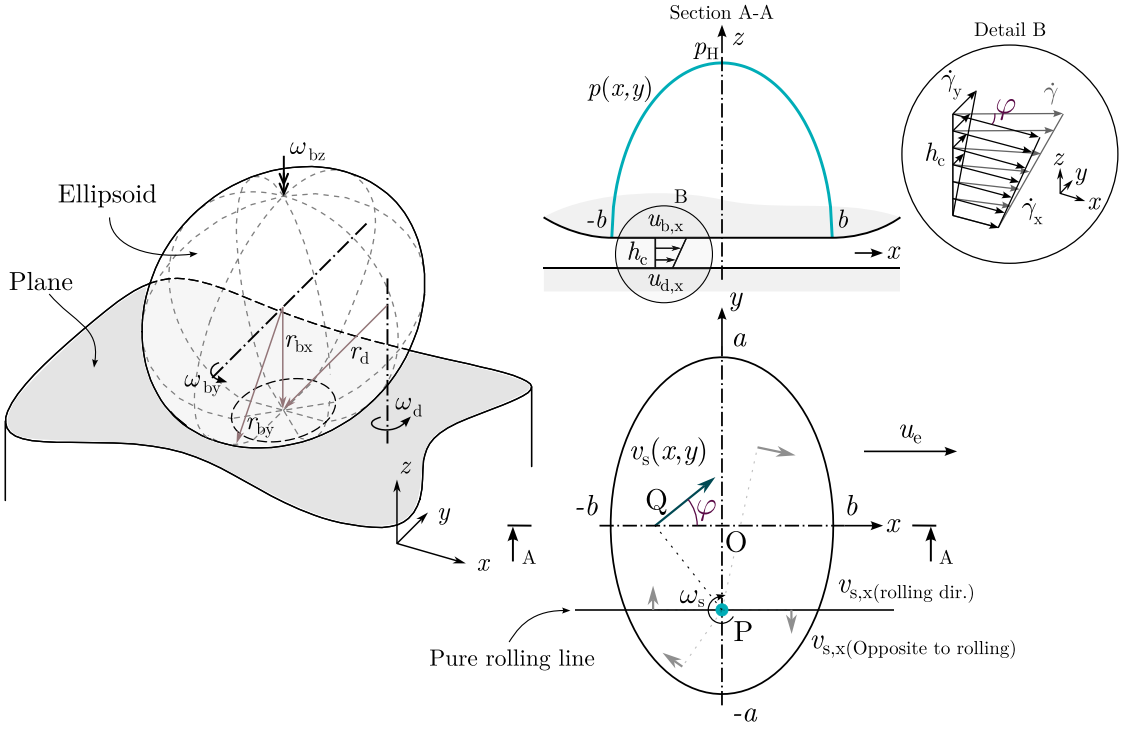

Fig. 1. Main parameters of the point contact.

literature [2], [24], [25], it can be proved that the spin pole position is not independent from longitudinal sliding.

$$\vec{\omega}_s \times \overrightarrow{PO} = \vec{v}_s(0,0) \rightarrow \left|\overrightarrow{PO}\right| = \frac{\vec{v}_s(0,0)}{\vec{\omega}_s} \tag{2}$$

$$\vec{v}_s(x,y) = \vec{\omega}_s \times \overrightarrow{PQ} = \vec{\omega}_s \times \left(\overrightarrow{PO} + \overrightarrow{OQ}\right) \tag{3}$$

2.2. Isothermal traction calculation

In the EHL regime, friction is caused by shearing of the fluid film confined in the contact interface. Hence, friction force can be calculated by integrating the shear stress across the contact area. The non-Newtonian shear stress τ in the lubricant is a function of the strain rate $\dot{\gamma}$, which depends on the sliding speed $v_s(x,y)$ and the non-Newtonian viscosity $\eta_G(p,\theta,\ \dot{\gamma})$. Furthermore, if the limiting shear stress coefficient Λ is considered, fluid pressure $p(x,y)$ affects the maximum traction attainable [29]. Therefore, local fluid behaviour is limited by the relationship between shear rate and pressure distributions. As the rheology of the lubricant is modelled by means of the Carreau non-Newtonian equation [30], the general mathematical formulation for traction prediction in a isothermal EHL contact is shown in Eq. 4.

$$\begin{aligned}\mu_x &= \frac{1}{F_n}\iint_{A_H} \tau_x \cdot dA_H \\ &= \frac{1}{F_n}\int_{-b}^{b}\int_{-a}^{a} \min\left(\dot{\gamma}\cdot\eta_L \cdot \left[1+\left(\frac{\eta_L\cdot\dot{\gamma}}{G}\right)^2\right]^{\frac{n-1}{2}}, \Lambda\cdot p\right)\cdot\cos\varphi\cdot dx\cdot dy\end{aligned} \tag{4}$$

where η_L is the low shear rate viscosity under constant temperature and local pressure calculated with the improved Yasutomi model [31], [32]; n and G are the Carreau's exponent and shear modulus, respectively; and F_n is the applied normal load. Since local sliding vectors $v_s(x,y)$ are no longer aligned with the rolling motion, the shear strain has two components, $\dot{\gamma}_x$ and $\dot{\gamma}_y$, which are aligned with the principal axes. These two terms must be considered when computing generalized viscosity with the Carreau expression and shear stresses in Eq. 4, where the absolute value of the local shear rate is $\dot{\gamma}^2 = \dot{\gamma}_x^2 + \dot{\gamma}_y^2$. Nevertheless, it is important to highlight that the φ angle in Fig. 1 denotes the direction of the local sliding vector, and should thus be considered in calculating the traction reaction in the main rolling direction. Since the shear stress across the film was assumed constant, the Couette flow shear strain rate may be considered as $\dot{\gamma}_x(x,y) = \partial u_x/\partial z \approx v_{s,x}(x,\ y)/h_c$. Fig. 2 depicts the relationship between sliding speed (shear strain rate) and shear stress distributions, with respect to the spin pole position.

2.3. Contact temperature determination

In Eq. 4, film thickness and viscosity are evaluated at constant inlet (θ_{in}) and contact temperatures (θ_c), both equal to the oil bath temperature θ_0. When computing oil film thickness, Chittenden's equation [27] can be updated to include thermal effects [23], shear thinning [15], and/or spinning effects [33]. However, the reduction of the central oil film thickness is negligible in spinning contacts, as recent experimental evidence has shown [33], [34]. Nonetheless, local shear stress distribution affects contact temperatures and therefore the traction coefficient is modified by spin. To overcome this, the rise in lubricant temperature within the contact is calculated by combining the energy equation in the lubricant film central plane with the point heat source integration method by Carslaw and Jaeger [35]. For any point Q in the contact region, the temperature of the film is calculated assuming that the heat is only conducted in the z-direction, and convection from the oil is neglected. Applying heat balance to the contact interface, the mid film temperature distribution can thus be expressed as:

$$\begin{aligned}\Theta_f(x,y,z) &= \Theta_{b,1} + \iint_{A_H} \alpha\cdot\dot{q}\cdot\left[R_{fl,1} + R_f\right] dA_H \\ &= \Theta_{b,2} + \iint_{A_H} (1-\alpha)\cdot\dot{q}\cdot\left[R_{fl,2} + R_f\right] dA_H\end{aligned} \tag{5}$$

where θ_b is a constant value representing the bulk temperature of the solid; α is the heat partitioning coefficient; $\dot{q}$ is the heat source of arbitrary shape due to the local fluid shear distribution calculated as $\dot{q}(x,y) = \tau(x,y)\cdot v_s(x,y)$; and R_{fl} and R_f are the thermal resistances for flash temperature rise and fluid heating, respectively. The former is computed from the analytical solution for quasi-steady state surface temperature distribution due to a moving heat source $\dot{q}(x,y)$ in a semi-infinite homogeneous medium. The latter can be derived by applying the energy equation and Fourier's law to a given lubricant differential area. Both solutions are presented in Eq. 6 (flash temperature rise) and 7 (fluid heating):

$$R_{fl,i}(x,y) = \frac{1}{2\cdot\pi\cdot K_i\cdot\sqrt{x^2+y^2}}\exp\left(-\frac{u_e}{2\cdot\chi_i}\cdot\left(\sqrt{x^2+y^2}-x\right)\right) \tag{6}$$

$$R_f(z) = \frac{1}{2\cdot K_{oil}}\cdot\left(\frac{h_c}{2}-z\right) \tag{7}$$

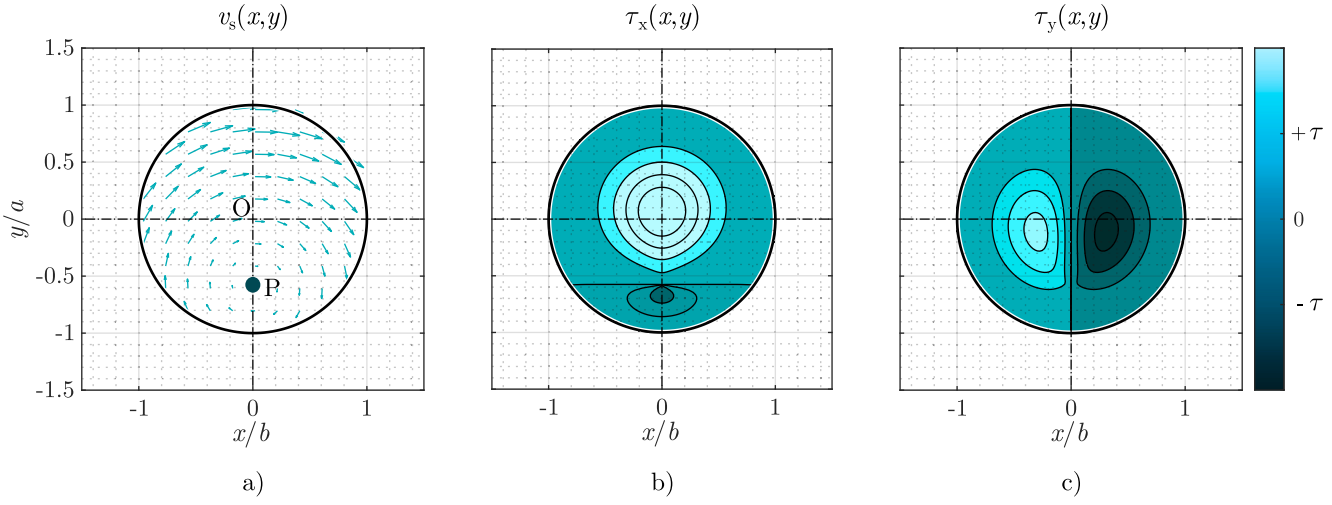

Fig. 2. a) Sliding speed distribution on the contact interface for SRR > 0%, b) shear stress distribution in the x-direction, and c) shear stress distribution in the y-direction.

where K_i is the thermal conductivity of the solid and χ_i the thermal diffusivity. Although a constant and equal heat partitioning of $\alpha = 0.5$ has been assumed in the interfaces due to both components being made of the same material, a range of heat partitioning between 0.4 and 0.6 has been considered. The traction results showed a 10% difference and the maximum deviation in traction do not exceed 0.007. Therefore, the bulk temperature of the solids is equal to that of the oil bath θ_0, and is thus simplified. In such conditions the fluid temperature distribution in the mid plane can be computed as a space convolution between $\dot{q}(x', y')$ and $R(x - x', y - y')$, which can be solved by FFT methods [36] after discretization on a uniform grid [37].

2.4. Contact power loss and efficiency

While traction is determined by the sliding components in the x-direction $\dot{\gamma}_x$, the term in the transverse direction (y-direction) still contributes to energy dissipation. Therefore, those interfaces subjected to an additional spin motion cause power loss, as expressed in Eq. 8. All sliding vectors generate power losses regardless of the vector direction, and hence the φ angle and the sliding component sign are not considered the equation.

$$P_{loss} = \iint_{A_H} |v_s| \cdot |\tau_x| \cdot dA_H = \int_{-b}^{b} \int_{-a}^{a} |v_s| \cdot \left| \min\left(\dot{\gamma} \cdot \eta_L \cdot \left[1 + \left(\frac{\eta_L \cdot \dot{\gamma}}{G} \right)^2 \right]^{\frac{n-1}{2}}, \Lambda \cdot p \right) \right| \cdot dx \cdot dy \quad (8)$$

From this definition, the contact efficiency can be readily determined, which is an indicator of the amount of power dissipated due to spinning speed with respect to useable tractive power: $P_{in} = T_{in} \cdot \omega_{in}$ and $P_{out} = F_n \cdot \mu_x \cdot u_{out}$.

Two sources of power loss can be distinguished in contacts with these kinds of kinematics: spin and longitudinal sliding losses. Longitudinal sliding losses increase in line with the slide to roll ratio (*SRR*), while spinning losses are predominant in low *SRR* conditions. Eq. 9 (longitudinal sliding) and Eq. 10 (spinning) determine the efficiency of these loss sources. The product between both efficiencies determines the global contact efficiency $Ef = Ef_{SRR} \cdot Ef_{spin} = 1 - (P_{loss}/P_{in})$.

$$Ef_{SRR} = \frac{F_t \cdot u_{out}}{F_t \cdot u_{in}} \quad (9)$$

$$Ef_{spin} = 1 - \frac{P_{loss} - P_{loss,SRR}}{P_{in}} \quad (10)$$

2.5. Calculation procedure

Fig. 3 sets out the procedure to determine the variables governing traction, which are as follows:

1. Determine input variables of the model considering the mechanical properties, geometries, disposition, and speed of the components, together with the supply temperature and the rheological properties of the lubricant.
2. Determine contact interface size and contact pressure distribution by means of the Hertzian contact model.
3. Calculate sliding speed distribution for imposed longitudinal sliding conditions.
4. Determine film thickness and shear strain rate distribution.
5. Calculate viscosity distribution in the contact region based on pressure, temperature, and kinematics.
6. Determine shear stresses and integration of shear stresses to calculate traction load.
7. Calculate changes in temperature distribution due to shearing of the lubricant fluid film.

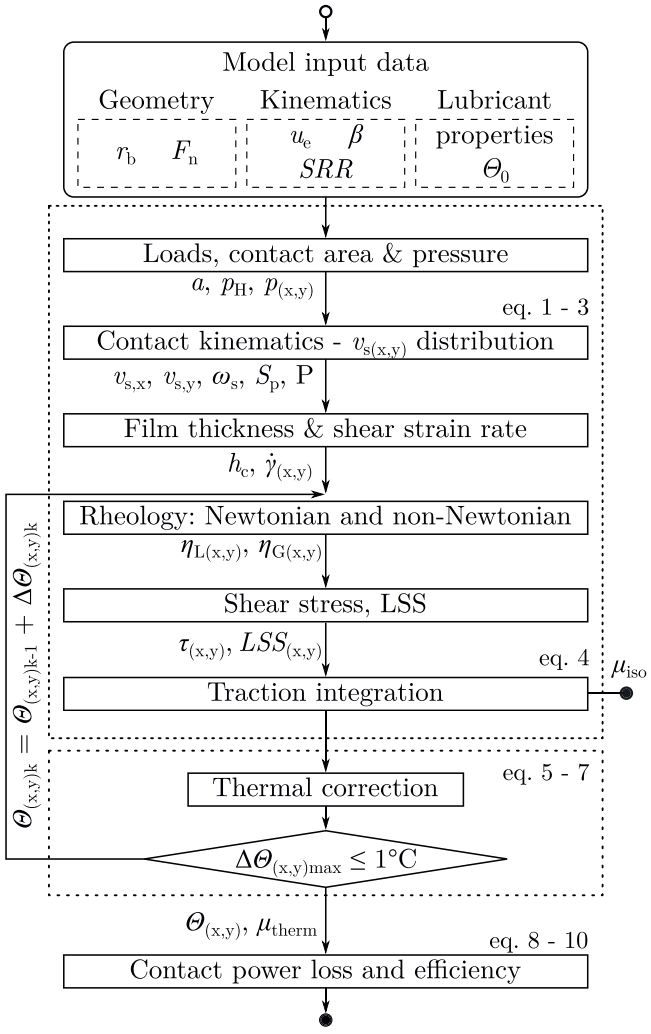

Fig. 3. Semi-analytical traction prediction model.

8. Repeat operations 5, 6, and 7, updating the contact temperature distribution until stabilized ($\Delta\Theta(x,y)_{max} \leq 1°C$).
9. Determine contact efficiency based on power losses and output power.

3. Case study

Three case studies were defined to analyse the impact of contact interface size on the traction coefficient of rolling, sliding, and spinning contacts under comparable conditions. For that purpose, the component disposition shown in Fig. 4 was considered, which is a generalization of the spinning contact types by Loewenthal [9].

Fig. 4 clearly shows that the rolling speed of the disc in the centre of the contact interface is $u_d = \omega_d \cdot r_d$, while the speed of the ball depends on the tilting angle, with $u_b = \omega_b \cdot r_b \cdot \cos(\beta)$. Thus, the overall rolling and sliding speeds can be calculated as $u_e = u_b + u_d/2$ and $v_s = u_b - u_d$, respectively, and the dimensionless longitudinal sliding (known as slide to roll ratio) is defined as $SRR = v_s/u_e$. However, the local fluid condition is affected by spinning motion, as the rotational speed of the disc and the ball are not equal. Therefore, the spinning speed is given by Eq. 11:

$$\vec{\omega}_s = \vec{\omega}_d + \vec{\omega}_b \cdot \sin(\beta) \quad (11)$$

where ω_b and ω_d are the rotational speed of the ball and the disc, respectively, and β is the tilting angle of the rotation axis of the ball.

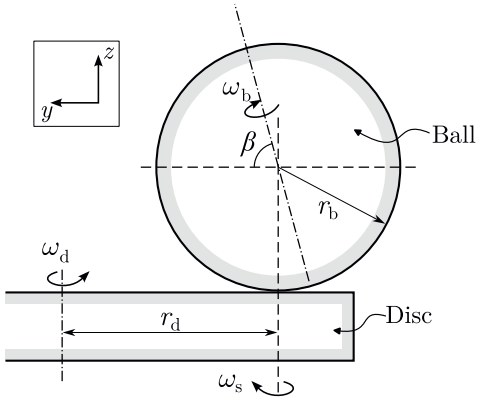

Fig. 4. A ball on disc disposition in which spinning motion may be controlled by the β angle.

To determine the traction coefficient under different contact scale and spinning speed conditions, the entrainment speed, contact pressure, and supply temperature of the lubricant were maintained constant by changing the normal load and disposition of the components. Three test cases were studied, as described below. The testing conditions are detailed in Table 1.

- Case 1 was designed to determine the accuracy of the model. To this end, the model results were compared to experimental rolling and sliding traction measurements with spin published in the literature [18]. The no spin condition ($\beta = 0°$) was measured for a different contact scale condition ($r_b = 12.5$ mm).
- Case 2 aimed to identify the behaviour of variables governing traction by changing both spinning speed and interface size, and observe the effect on the traction coefficient. Tests were carried out under equal spin to roll ratio, maintaining an equal relationship between the spinning speed and the Hertzian contact radius.
- Case 3 was performed at a fixed spinning speed under all conditions. The only variable changed was the contact interface size.

The properties of the materials used in the analysis are shown in Table 2. Both the ball and disc were made of AISI 52100 (100Cr6) through hardened steel, and the lubricant was Shell T9 [38].

4. Results and discussion

4.1. Comparison of model and experimental results

The correlation between the results obtained from the traction prediction model and published data [18] is illustrated in Fig. 5. The figure clearly shows that the model accurately reflects the general trends of the experimental traction coefficient data. The maximum difference in traction coefficient does not exceed 0.014, while the average difference is only 0.005.

Table 1
The modelled working conditions for each case study.

Parameter	1	2	3
u_e	2 m/s	2 m/s	2 m/s
r_b	[12.5 mm* , 80 mm]	40 mm	20 mm
r_d	50 mm	50 mm	50 mm
β	[0°, 86°, 88°, 88.5°]	84°	[84°, 87°, 88.5°]
F_n	1500 N	[155.3, 621, 2484.2] N	[155.3, 621, 2484.2] N
p_H	0.845 GPa	1 GPa	1 GPa
a	0.92 mm	[0.27, 0.54, 1.09] mm	[0.27, 0.54, 1.09] mm
Θ_0	30 °C	30 °C	30 °C
SRR	[− 45–45%]	[0–50%]	[0–50%]
$\omega_s(SRR_{x,0} = 0\%)$	[0, 397, 755, 991] rad/s	[991, 495, 248] rad/s	991 rad/s

*the 12.5 mm ball was considered only for the no spin condition ($\beta = 0$ °)

Table 2
Solid and lubricant properties.

Steel AISI 52100[39,40]		
Elasticity modulus	E	210 GPa
Poisson's ratio	ν	0.3
Density	ρ	7800 kg/m^3
Thermal conductivity	K	21 W/mK
Specific heat	c	460 J/kgK
Shell T9[38,41]		
Viscosity ($\theta = 40$ °C)	η_0	0.008 Pa·s
Density ($\theta = 40$ °C)	ρ_0	872 kg/m^3
LSS coefficient	Λ	0.083
Thermal conductivity	K_{oil}	0.1114 W/mK
Temperature at glass transition	Θ_{g0}	-83.2 °C
Viscosity at glass transition	η_g	$1{\cdot}10^{12}$ Pa·s
Yasutomi parameters	A1	188.86 °C
	A2	0.719 GPa^{-1}
	b1	8.2 GPa^{-1}
	b2	-0.5278
	C1	16.09
	C2	17.38 °C
Shear modulus	G	7 MPa
Power law exponent	n	0.35

- Increasing the spin (β angle) results in a reduction in traction across all slide to roll ratio conditions.
- Differences in traction between the three spinning speed conditions are greater under low longitudinal sliding conditions, since spin motion has a more significant impact at this working range.
- Under high longitudinal sliding conditions, the results of the traction coefficient converge on the same value regardless of the spinning speed condition. This is particularly evident in the $SRR = -45\%$ condition for both experimental and numerical results. It has to be remarked that the $\beta = 0°$ condition does not converge to the same traction value for high longitudinal sliding conditions since the experimental results from the literature were carried out under a different scale condition ($r_b = 12.5$ mm). As a result, variations in thermal behaviour are expected, leading to differences in the obtained results. These findings align with similar observations in the literature, where it has been demonstrated that interfaces with smaller sizes exhibit higher traction coefficients due to lower thermal heating [12].
- Under positive longitudinal sliding conditions, the traction coefficient values do not completely converge in high sliding conditions as happens for the negative sliding condition (e.g., 88° and 88.5°). This

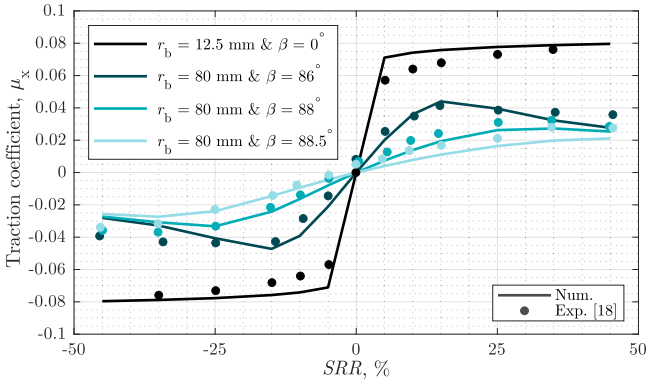

Fig. 5. Comparison between model and published results.

is a result of the variation of the spin speed as a function of longitudinal sliding, which occurs due to the adjustment of the speed of the components to maintain a constant input speed across different longitudinal sliding speeds. Therefore, the spin pole position at positive and negative longitudinal sliding conditions cannot be directly compared. The spin pole locations are shown subsequently for both longitudinal sliding directions, which highlights the differences in traction under positive and negative longitudinal sliding conditions.

Fig. 6 depicts the sliding speed distribution for the three spinning conditions at $SRR = -45\%$ and $SRR = 45\%$.

- In negative longitudinal sliding conditions, the spin pole P moves in the positive y-direction, while in positive longitudinal sliding, it moves in the negative y-direction. The differences in spin pole distance between positive and negative longitudinal sliding conditions occur because the rotational speed of the disc and ball are adjusted to maintain a constant entrainment speed when the longitudinal sliding speed is changed. As a result, the spinning speed is no longer constant as a function of longitudinal sliding.
- The spinning speed is greater under positive longitudinal sliding conditions because the speed of the ball is accelerated, bringing the spin pole closer to the contact centre. Since the spin pole remains inside the Hertzian contact region for the $SRR = 45\%$ the traction coefficient values do not converge in an equal value.

The obtained traction trends are in accordance with the observations of Ehret et al. [10]. They found that the traction coefficient is affected when the spin pole is inside the Hertzian contact region. This, together with the spin pole positions shown in Fig. 6, can explain why the traction coefficients converge at $SRR = -45\%$, while at $SRR = 45\%$ the traction coefficients remain different. The spin pole of the $\beta = 88.5^\circ$ condition is still inside the Hertzian contact region, and thus the obtained traction coefficient is lower than the traction coefficient of the other two conditions.

4.2. Equal spin to roll ratio

The isothermal and thermally corrected traction curves calculated under equal spin to roll ratio conditions are shown in Fig. 7. For that purpose, both spin speed and contact interface size were changed in each condition, maintaining an equal relationship between the three conditions. The isothermal curves show similar trends under the three conditions, which indicates that the spin to roll ratio completely characterizes the contact behaviour. In contrast, the thermally corrected

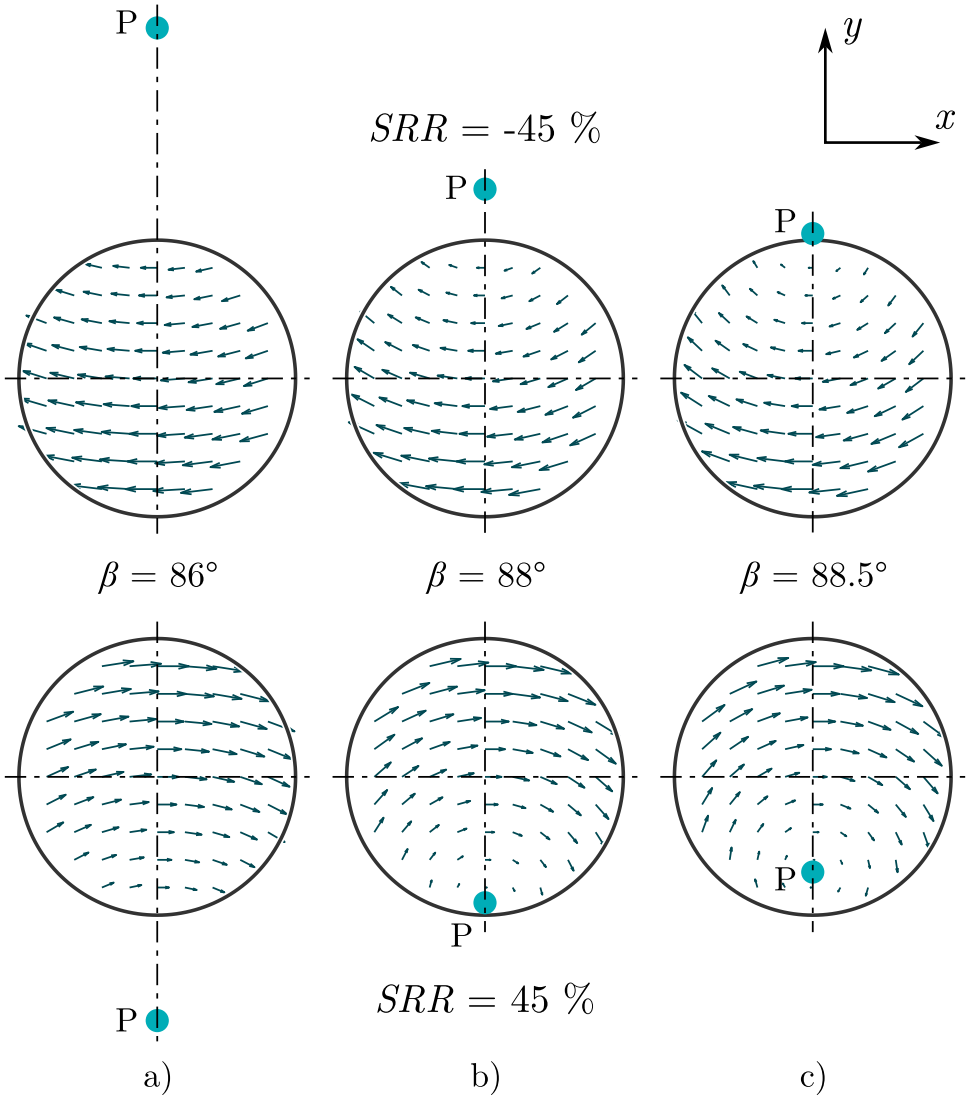

Fig. 6. Sliding speed distribution on the contact surfaces for SRR = −45% (top) and SRR = 45% (bottom) when a) β = 86°, b) β = 88° and c) β = 88.5°.

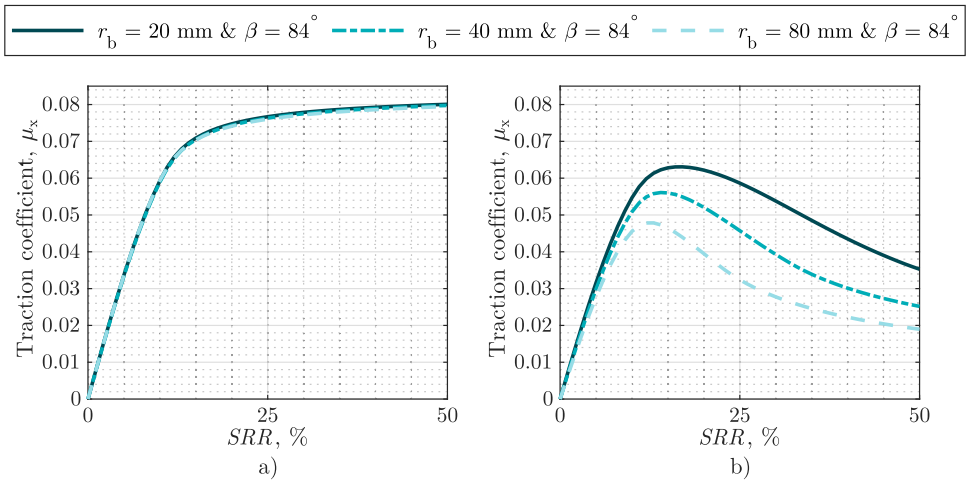

Fig. 7. Traction coefficient for equal spin to roll ratio conditions in a) isothermal and b) thermal conditions.

traction results present a lower traction coefficient as the contact scale increases. These differences are more considerable in high longitudinal sliding conditions. In addition, the thermally corrected traction shows that the maximum traction coefficient decreases as the contact interface size increases.

Fig. 8 illustrates kinematic parameters (spin speed, spin to roll ratio, spin pole position, and dimensionless spin pole position (P/a)) as a function of longitudinal sliding.

- The spinning speed increases together with longitudinal sliding for the three contact radius conditions. The variation in spin speed results from the changes in the rotational speed of the disc and the ball, i.e., maintaining the entrainment speed constant while longitudinal sliding changes has an effect on the spinning speed. Nevertheless, the variation in the spinning speed is proportional to the contact radius as a function of longitudinal sliding in the three conditions.
- The spin to roll ratio is equal for the three conditions analysed, since the large interface has low spinning speed and vice versa. The variation in spin to roll ratio with respect to longitudinal sliding is also equal in the three scale conditions, which means that the traction results in isothermal conditions are comparable.
- As the spin speed varies across the three scale conditions, the position of the spin pole differs depending on the longitudinal sliding, as determined by Eq. 2. In the smaller-sized interface, the distance between the spin pole and the centre of the contact is smaller compared to the larger interface. Consequently, when the spin pole resides on the boundary of the contact interface, the longitudinal sliding is equivalent in all three scale conditions. Hence, the dimensionless spin pole position remains consistent across all three conditions (Fig. 8d).

Fig. 9 plots the sliding speed, isothermal shear stress, temperature rise, and thermally corrected shear stress in the rolling direction on the contact interface when *SRR* equals 10%. The sliding speed distribution indicates that the position of the spin pole is equal in the three scale conditions. This corresponds with Fig. 8d, in which the relationship between the spin pole position and the interface radius is equal. Therefore, it can be seen that since the relationship between the

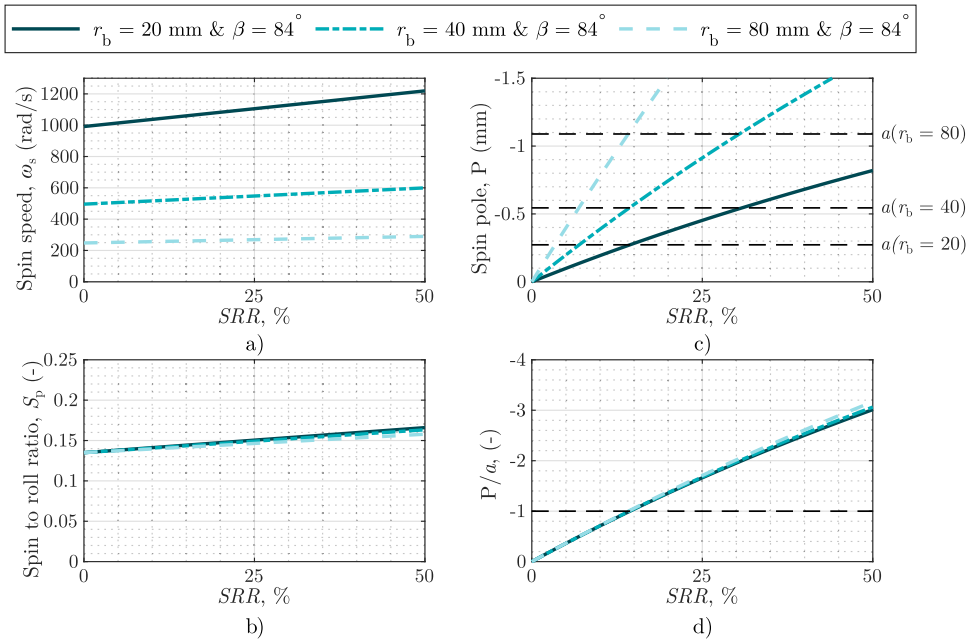

Fig. 8. a) Spinning speed, b) spin to roll ratio, c) spin pole position, and d) relationship between spin pole and interface size as a function of longitudinal sliding for three contact interface conditions under equal spin to roll ratio conditions.

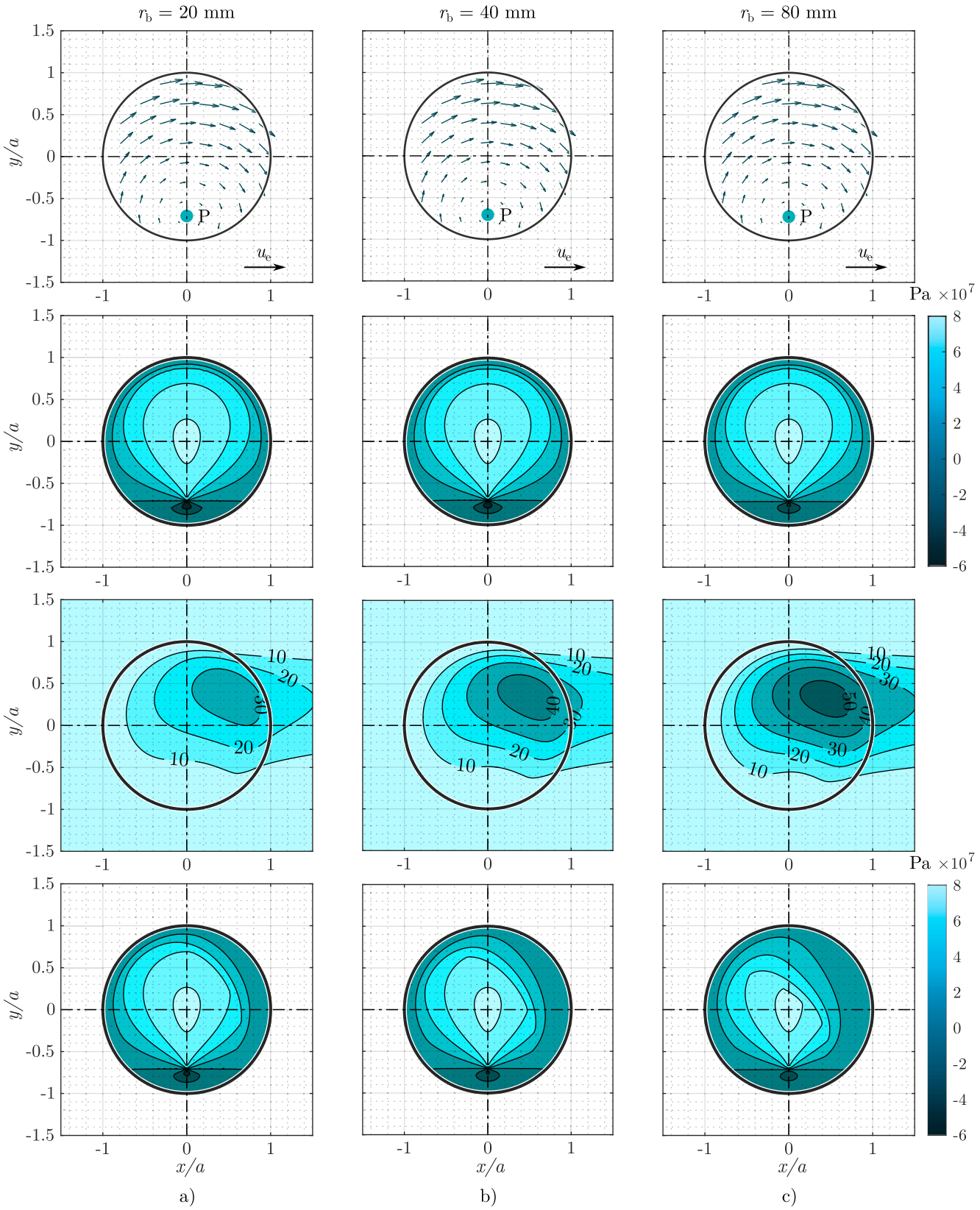

Fig. 9. (From top to bottom) Surface sliding speed distribution, isothermal shear stresses in the rolling direction, temperature rise distribution and thermal shear stress under equal spin to roll ratio conditions for SRR = 10% and a) $r_b = 20$ mm, b) $r_b = 40$ mm, and c) $r_b = 80$ mm.

spinning speed and contact interface radius is equal, the sliding speed values across the contact interface are equal, i.e., $v_s(x/a, y/a)_{R20} = v_s(x/a, y/a)_{R40} = v_s(x/a, y/a)_{R80}$. As the sliding speed distribution is equal across the contact interface, the viscosity distribution would also be similar in the three scale conditions. Therefore, the isothermal shear stresses are equal in the three scale conditions as can be seen in the second row of Fig. 9.

The third row of Fig. 9 depicts the temperature rise distribution on the mid plane generated by the shearing of the lubricant. The figure clearly shows that the temperature distribution coincides with the sliding speed distribution. On the one hand, the temperature at the outlet increases as a result of the rolling direction of the components in contact. On the other hand, the temperature rise in the negative y-region is smaller than in the positive y-region. This behaviour is a result of the spin motion. Since there is no heat generation in the spin pole position (no sliding speed) the temperature increase near this region is lower.

The corrected temperature distribution decreases the viscosity of the lubricant, and thus changes in shear stresses are expected. The bottom row of Fig. 9 presents the thermally corrected shear stress distribution in the rolling direction. It can be observed that the shear stresses of the large interface are lower than those of the small interface. Hence, the traction coefficient of the large interface can be expected to be lower than the low scale, as also reported in Fig. 7b.

This case study reveals that the spin to roll ratio completely characterizes the kinematic behaviour of the spinning circular contacts. Nevertheless, the traction coefficient is influenced by the scale effect, since the interface size affects the thermal behaviour of the contact. Similar traction behaviour was stated in the literature for traction trends without considering spin speed in the contact [12–14], where lower traction coefficient was achieved for large size contacts, mainly due to thermal effects.

4.3. Equal spinning speed

The traction curves for the equal spinning speed and variable contact interface size conditions are plotted in Fig. 10. The β angle was adapted to achieve the same spinning speed in the three scale conditions. In this case, the isothermal analysis presented differences in traction between the three scale conditions, which reveals that the source of these differences is not only the thermal behaviour. Nevertheless, differences in the traction coefficient increased in the thermally corrected traction curves, which shows that the larger the contact interface the lower the traction coefficient.

The main kinematic parameters as a function of longitudinal sliding are reported in Fig. 11. The spinning speed is equal in the three scale conditions, therefore, the spin to roll ratio is no longer equal since the contact size has changed. In addition, since the spinning speed is equal, the position of the spin pole as a function of longitudinal sliding is equal for the analysed three conditions. Hence, the spin pole is inside the Hertzian contact region for different longitudinal sliding range at each scale, as shown in Fig. 11c (the greater the interface size the spin pole is inside for a wider range). As a result, the dimensionless spin pole position is no longer equal for the three scale conditions.

Fig. 12 depicts the sliding speed distribution on the contact interface for $SRR = 10\%$. The figure clearly shows that the spin pole position changes in proportion to the interface size, which corresponds to Fig. 11c, in which the spin pole position was shown to be equal in the three conditions. Hence, since the spinning speed is equal, the sliding speed values at the contact boundaries are different, because the speed of the large size interface is higher. In this case, the sliding speed distribution is related as $v_s(x, y)_{R20} = v_s(x, y)_{R40} = v_s(x, y)_{R80}$. Moreover, as the spin pole is closer to the contact interface centre for the large scale condition, more sliding appears in the opposite direction to rolling, and thus, traction is affected.

The second row of Fig. 12 shows the isothermal shear stress distribution on the contact interface. As expected, more shear stresses can be observed in the negative x-direction of the largest interface, and thus less traction can be expected after the integration. This is in agreement with the results depicted in Fig. 10, where the large size interface is the one with the lowest traction coefficient.

The distribution of temperature rise on the contact interfaces is reported in the third row of Fig. 12. As expected, the rise in temperature is greater on the large interface than the small one, which leads to a larger decrease in viscosity, and thus traction. Since the spin pole is closer to the centre of the contact interface in the largest contact size, the temperature distribution changes accordingly. This is evidenced by a low temperature rise near the spin pole, which can be attributed to the absence of sliding at that particular point. On the other hand, it also indicates that an increase in temperature corresponds to an increase in the size of the contact interface.

The bottom row of Fig. 12 shows the distribution of thermally corrected shear stress distribution in the rolling direction for the three scale conditions. The findings indicated a greater decrease of the shear stresses on the largest contact interface, consequently resulting in a substantially greater decrease in the traction coefficient.

Shear stresses in the positive direction lead to an increase in the traction coefficient, while shear stresses in the negative direction result in a decrease. It can thus be concluded that in the integration process, the shear stresses in the positive direction are cancelled by the shear stresses in the negative, which has a resultant effect on the traction coefficient. Nevertheless, all these shear stresses generate energy dissipation, which increases the contact power loss, thereby decreasing the

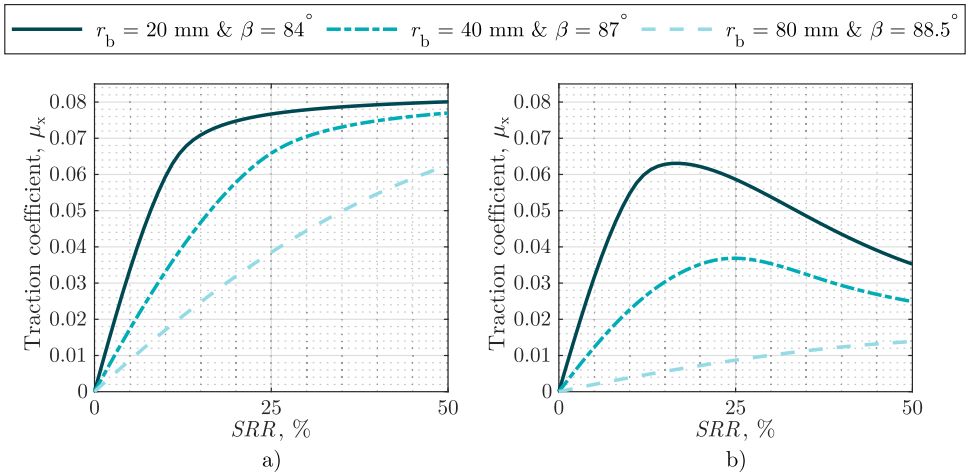

Fig. 10. Traction coefficient for equal spinning speed conditions in a) isothermal and b) thermal conditions.

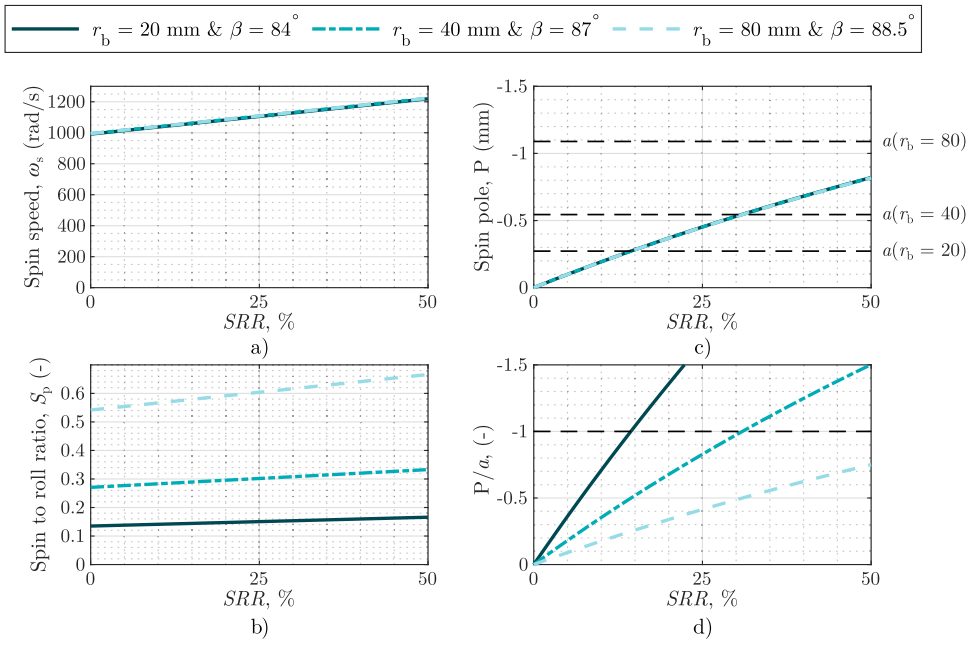

Fig. 11. a) Spinning speed, b) spin to roll ratio, c) spin pole position, and d) dimensionless spin pole position as a function of longitudinal sliding for equal spinning speed conditions.

efficiency.

4.4. Contact efficiency results

The contact efficiencies were also studied so as to determine the optimum working condition of each contact condition. Although traction is affected by the scale effect, contact efficiency is solely dependent upon spin to roll ratio as shown in Fig. 13a. The figure illustrates the dramatic increase in efficiency as a function of longitudinal sliding until an optimum point is reached. From that condition forward, the efficiency decreases gradually while *SRR* increases. This trend is determined by two sources of power loss—spin and longitudinal sliding. Each of these sources of loss affect different regions as stated in Eq. 9 and Eq. 10. Spinning efficiency, on the one hand, increases rapidly with longitudinal sliding reaching 100% at SRR = 15%. This corresponds to the condition when the spin pole is positioned within the boundaries of the Hertzian contact region (Fig. 13b). On the other hand, increasing longitudinal sliding leads to a gradual decrease in longitudinal sliding efficiency (Fig. 13c).

While Ehret et al. [10] mentioned that spin affects when the spin pole is inside the Hertzian contact region, it has been found that the maximum contact efficiency occurs when the spin pole remains within the contact region under the analysed conditions. It should be noted that he overall efficiency decreases significantly when the spin pole reaches the contact boundaries, resulting in higher longitudinal sliding losses compared to when it is within the Hertzian contact region as shown in Fig. 13a.

In the case of equal spinning speed, the contact efficiency as a function of longitudinal sliding is plotted in Fig. 14a. The figure shows that the efficiency of the large size interface is considerably lower than the other two scale conditions. In addition, the maximum efficiency condition occurs under higher longitudinal sliding conditions for the large interface. Fig. 14b illustrates that the spinning efficiency is different for each scale condition, and is affected by the spin pole position. Since the spin pole is inside the Hertzian contact region in a wider range of longitudinal sliding for the large interface, the spinning efficiency is lower than the other two scale conditions. Nevertheless, since the longitudinal sliding is equal for all the scale conditions, its efficiency is equal for all three, as represented in Fig. 14c. These results indicate that to maximize efficiency under equal spinning speed conditions, it is preferable to use low scale contact interfaces. Newall et al. [20] and Verbelen et al. [42] also identified a decrease in efficiency, noting that higher conformity ratios on the contact (corresponding to a higher equivalent radius) led to lower efficiencies. However, these studies did not specifically correlate the efficiency decrease with the spin motion or spin pole position.

5. Conclusions

A simplified semi-analytical traction prediction model has been presented, which analyses the impact of spinning motion on the traction coefficient, while also considering the influence of interface size. The results demonstrate that the model adequately represents the spin induced traction trends with a maximum and mean difference in traction coefficient that do not exceed 0.014 and 0.005 respectively. Although the simplified nature of the model led to some differences between simulated and experimental results, the model has proved effective in obtaining rapid insights into traction not achievable by complex numerical models. Furthermore, contact efficiency was also analysed to determine how the contacts behave as a function of longitudinal sliding. The results of this study can contribute to the enhanced design of mechanisms which include rolling, longitudinal sliding, and spinning contacts. The main conclusions are as follows:

- The traction coefficient is affected by both spinning motion and interface size. The presented study has reported that the spin to roll ratio provides a comprehensive description of the kinematic conditions, as the longitudinal sliding where the spin pole is located within the contact boundaries remains consistent across all conditions. However, it has been observed that decreasing the contact interface size mitigates the impact of spin motion. At equal spinning speed conditions, low sized interfaces show less sliding across the contact interface, therefore, less shear thinning of the lubricant and thermal effects of the fluid occur. Consequently, optimizing the traction coefficient and contact efficiency may be achieved through the utilization of smaller interfaces.
- The spin to roll ratio properly represents the kinematic behaviour of the contact interface, and thus, traction under an equal spin to roll

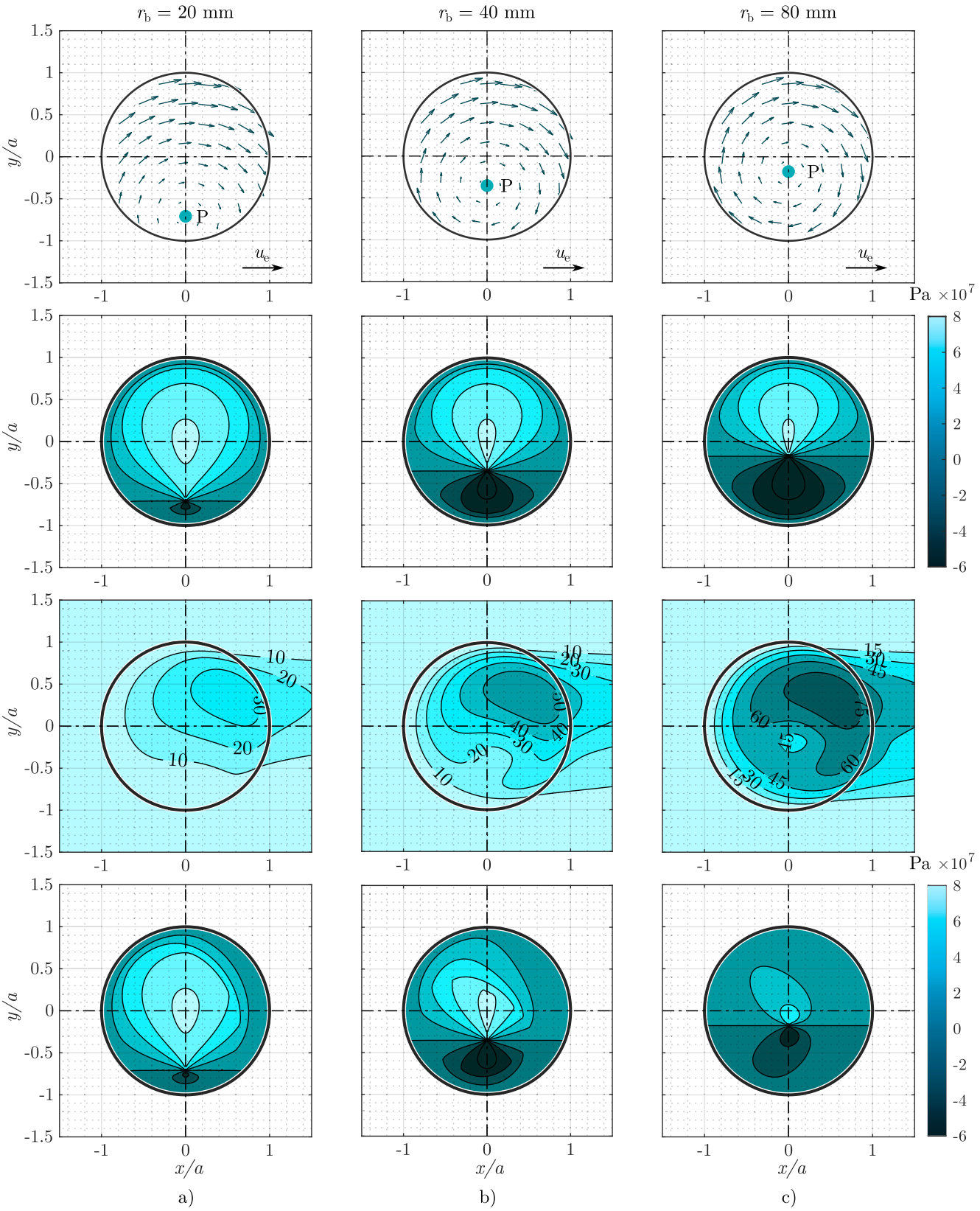

Fig. 12. (From top to bottom) Surface sliding speed distribution, isothermal shear stresses in the rolling direction, temperature rise distribution and thermal shear stress under equal spinning speed conditions for SRR = 10% and a) r_b = 20 mm, b) r_b = 40 mm, and c) r_b = 80 mm.

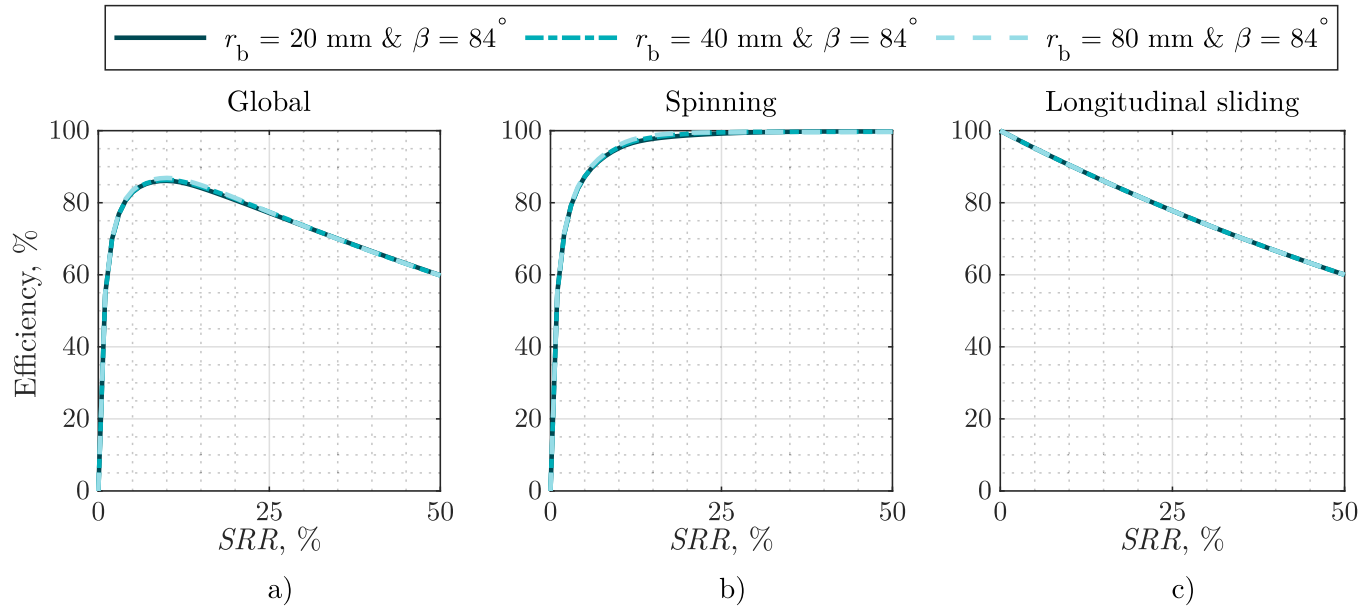

Fig. 13. Contact efficiency for equal spin to roll ratio as a function of longitudinal sliding: a) global efficiency b) spinning efficiency and c) longitudinal sliding efficiency.

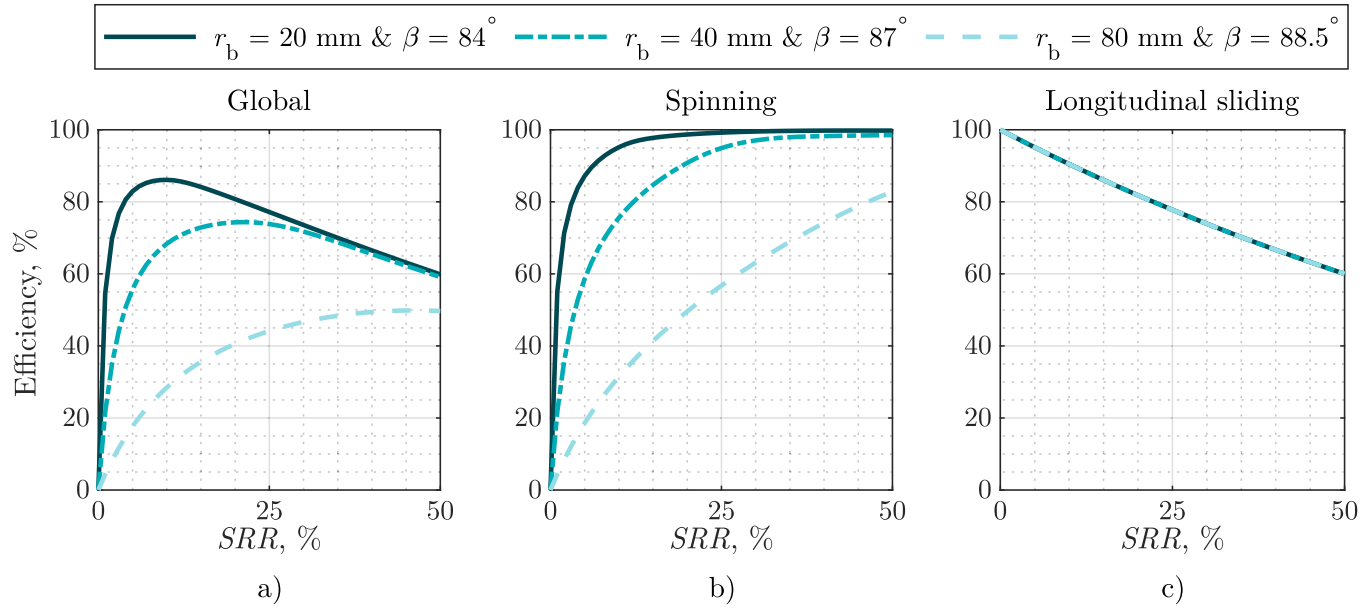

Fig. 14. Contact efficiency for equal spinning speed as a function of longitudinal sliding: a) global efficiency b) spinning efficiency and c) longitudinal sliding efficiency.

ratio is similar for different scale conditions under isothermal conditions. However, differences were found in the thermally corrected traction curve, since the interface size affects thermal behaviour. Large scale interfaces lead to a greater rise in temperature than small scale interfaces. As a result, the decrease in traction is greater for large interfaces.

- In equal spinning speed conditions, differences were observed between the contact sizes under isothermal conditions. Firstly, more shear thinning occurred in large scale interfaces due to the increased sliding speed on the surface. Secondly, these large interfaces reported higher shear stresses in the negative direction on the surface, since the spin pole is closer to the contact centre relative to the surface radius. However, it should be noted that the shear stresses below the spin pole act in the negative direction and do not contribute to enhancing traction.
- The integration of shear stresses in the rolling direction generates traction. Nevertheless, shear stresses in the negative direction cancel shear stresses in the positive, which leads to increased power losses. In addition, the shear stresses in the y-direction (transverse to rolling) do not generate traction load, but rather increase the energy dissipation, and hence power losses and efficiency. Larger interface sizes result in increased sliding in the negative or transverse direction to rolling, leading to higher energy dissipation. Consequently, both traction and contact efficiency are lowered as the contact interface size increases.

Spin speed and contact interface size are independently controlled in

the design of mechanisms such as toroidal continuously variable transmissions. While these parameters may vary during operation, they do so in a predetermined manner, and their operation is not actively controlled. The results presented in this paper would indicate that smaller surface sizes may be preferable in such mechanisms. In this way, transferable torque (traction) and efficiency of the transmission would be considerably improved.

In applications where working in low longitudinal sliding conditions is preferred, Fig. 14a demonstrates that smaller interfaces can result in a three-fold increase in efficiency. However, in applications where high longitudinal sliding is likely to occur, though, the scale has minimal impact on efficiency, as all contact sizes experience equal longitudinal sliding losses. Consequently, compromising other design aspects to reduce the contact radius may not be worthwhile, as it does not provide any efficiency benefit.

Declaration of Competing Interest

The authors declare the following financial interests/personal relationships which may be considered as potential competing interests. Authors report financial support and administrative support were provided by Mondragon Unibertsitatea Faculty of Engineering.

Data Availability

Data will be made available on request.

Acknowledgements

This project has received funding from the European Union's Horizon 2020 research and innovation programme under grant agreement No 820670.

Statement of Originality

As corresponding author, hereby confirm on behalf of all authors that the paper has not been published previously, that it is not under consideration for publication elsewhere, and that if accepted it will not be published elsewhere in the same form, in English or in any other language, without the written consent of the publisher.

References

[1] Dormois H, Fillot N, Vergne P, Dalmaz G, Querry M, Ioannides E, Morales-Espejel GE. First traction results of high spinning large-size circular EHD contacts from a new test rig: tribogyr. Tribology Trans 2009. https://doi.org/10.1080/10402000802105448.
[2] Tevaarwerk JL. A simple thermal correction for large spin traction curves. J Mech Des 1981. https://doi.org/10.1115/1.3254936.
[3] Echávarri-Otero J, de la Guerra Ochoa E, Tanarro EC, del Río López B. Friction coefficient in mixed lubrication: a simplified analytical approach for highly loaded non-conformal contacts. Adv Mech Eng 2017. https://doi.org/10.1177/1687814017706266.
[4] G.E. Morales-Espejel and A.W. Wemekamp, "An engineering approach on sliding friction in full-film, heavily loaded lubricated contacts," Proceedings of the Institution of Mechanical Engineers, Part J: Journal of Engineering Tribology, 2004. DOI: ⟨10.1243/1350650042794806⟩.
[5] Itagaki H. Method for estimating traction curves under practical operating conditions. Tribology Int 2020. https://doi.org/10.1016/j.triboint.2019.02.047.
[6] Meyer C. Reibung in hoch belasteten EHD-Wälzkontakten, PhD thesis. Leibniz Univ Hann 2010. https://doi.org/10.15488/7473.
[7] Machida H, Itoh H, Imanishi T, Tanaka H. Design principle of high power traction drive CVT. SAE Tech Pap 1995. https://doi.org/10.4271/950675.
[8] Novellis LD, Carbone G, Mangialardi L. Traction and efficiency performance of the double roller full-toroidal variator: a comparison with half- and full-toroidal drives. J Mech Des 2012. https://doi.org/10.1115/1.4006791.
[9] Loewenthal SH. Spin analysis of concentrated traction contacts. J Mech Transm Autom Des 1986. https://doi.org/10.1115/1.3260788.
[10] P. Ehret, F. Chevalier, D. Dowson, C.M. Taylor, H. Okamura, and T. Sano, "Traction in EHL Elliptical Contacts with Spin Conditions," Thinning Films and Tribological Interfaces, Proceedings of the 26th Leeds-Lyon Symposium on Tribology, 2000. DOI: ⟨10.1016/s0167–8922(00)80113–3⟩.
[11] Bergseth E, Zhu Y, Söderberg A. Study of surface roughness on friction in rolling/sliding contacts: ball-on-disc versus twin-disc. Tribology Lett 2020. https://doi.org/10.1007/s11249-020-01310-z.
[12] Liu HC. Scale and contact geometry effects on friction in thermal EHL: twin-disc versus ball-on-disc. Tribology Int 2020. https://doi.org/10.1016/j.triboint.2020.106694.
[13] D. Philippon, L. Martinie, and P. Vergne, Discussion on 'Scale and contact geometry effects on friction in thermal EHL: twin-disc versus ball-on-disc' by Liu, Zhang, Bader, Venner, Poll, Tribology International 154, 106694, 2021," Tribology International, 2021. DOI: ⟨10.1016/j.triboint.2021.106877⟩.
[14] H.C. Liu and G. Poll, "Reply to the Discussion by Philippon, Martinie, Vergne on 'Scale and Contact Geometry Effects in Thermal EHL: Twin-Disc versus Ball-on-Disc' by Liu, Zhang, Bader, Venner and Poll in Tribology International," Tribology International, 2022. DOI: ⟨10.1016/j.triboint.2022.108204⟩.
[15] Liu HC, Zhang BB, Bader N, Venner CH, Poll G. Simplified traction prediction for highly loaded rolling/sliding EHL contacts. Tribology Int 2020. https://doi.org/10.1016/j.triboint.2020.106335.
[16] S.Y. Poon, "Some Calculations to Assess the Effect of Spin on the Tractive Capacity of Rolling Contact Drives," Proceedings of the Institution of Mechanical Engineers, 1970. DOI: ⟨10.1243/pime_proc_1970_185_115_02⟩.
[17] H. Dormois, "Frottement dans les contacts EHD de grandes dimensions, role du pivotement," PhD Thesis. L'Institut National des Sciences Appliquées de Lyon, 2008.
[18] T. Doki-Thonon, "Thermal effects in elastohydrodynamic spinning circular contacts," PhD Thesis. L'Institut National des Sciences Appliquées de Lyon, 2012.
[19] J.D. Wheeler, "Non-Elliptical Point Contacts: the Torus-on-Plane Conjunction," PhD Thesis. L'Institut National des Sciences Appliquées de Lyon, 2016.
[20] Newall J, Lee A. Measurement and prediction of spin losses in the EHL point contacts of the full toroidal variator. Tribology Ser 2003. https://doi.org/10.1016/s0167-8922(03)80105-0.
[21] Popovici RI, Schipper DJ. Stribeck and traction curves for elliptical contacts: isothermal friction model. Int J Sustain Constr Des 2014. https://doi.org/10.21825/scad.v4i2.1042.
[22] R.I. Popovici, Friction in wheel - rail contacts, PhD Thesis. University of Twente, 2010. DOI: ⟨10.3990/1.9789036529570⟩.
[23] A. Arana, J. Larrañaga, and I. Ulacia, "Partial EHL friction coefficient model to predict power losses in cylindrical gears," Proceedings of the Institution of Mechanical Engineers, Part J: Journal of Engineering Tribology, 2018. DOI: ⟨10.1177/1350650118778655⟩.
[24] Tevaarwerk JL, Johnson KL. The influence of fluid rheology on the performance of traction drives. J Lubr Technol 1979. https://doi.org/10.1115/1.3453346.
[25] J.L. Tevaarwerk, "Traction calculations using the shear plane hypothesis," Proc. Of Leeds-Lyon Symposium on Tribology, 1979.
[26] F. Chevalier, "Modélisation des conditions d'alimentation dans les contacts élastohydrodynamiques ponctuels," PhD Thesis. Ecole Doctorale Mecanique, Energetique, Genie Civil, Acoustique (MEGA), 1996.
[27] R.J. Chittenden, D. Dowson, J.F. Dunn, and C.M. Taylor, "A Theoretical Analysis of the Isothermal Elastohydrodynamic Lubrication of Concentrated Contacts. II. General Case, with Lubricant Entrainment along Either Principal Axis of the Hertzian Contact Ellipse or at Some Intermediate Angle," Proceedings of the Royal Society A: Mathematical, Physical and Engineering Sciences, 1985. DOI: ⟨10.1098/rspa.1985.0015⟩.
[28] H. Moes, Lubrication and Beyond. University of Twente, 2000.
[29] Ndiaye SN, Martinie L, Philippon D, Devaux N, Vergne P. A quantitative friction-based approach of the limiting shear stress pressure and temperature dependence. Tribology Lett 2017. https://doi.org/10.1007/s11249-017-0929-2.
[30] Carreau PJ. Rheological equations from molecular network theories. Trans Soc Rheol 1972. https://doi.org/10.1122/1.549276.
[31] Vergne P, Bair S. Classical EHL versus quantitative EHL: a perspective part I-real viscosity-pressure dependence and the viscosity-pressure coefficient for predicting film thickness. Tribology Lett 2014. https://doi.org/10.1007/s11249-014-0302-7.
[32] S. Bair, C. Mary, N. Bouscharain, and P. Vergne, "An improved Yasutomi correlation for viscosity at high pressure," Proceedings of the Institution of Mechanical Engineers, Part J: Journal of Engineering Tribology, 2013. DOI: ⟨10.1177/1350650112474394⟩.
[33] A. Porras-Vazquez, "Lubricant starvation in elastohydrodynamic large-size spinning contacts," PhD Thesis. L'Institut National des Sciences Appliquées de Lyon, 2020.
[34] Porras-Vazquez A, Philippon D, Fillot N, Vergne P, Devaux N, Lafarge L, Morales-Espejel GE. An experimental approach to evaluate film thickness in starved large-size spinning contacts. J Tribology 2022. https://doi.org/10.1115/1.4054863.
[35] Carslaw HS, Jaeger JC. Conduction of Heat In Solids. Oxford University Press; 1959.
[36] Liu Y-C, Wang H, Wang W-Z, Hu Y-Z, Zhu D. Methods comparison in computation of temperature rise on frictional interfaces. Tribology Int 2002. https://doi.org/10.1016/s0301-679x(02)00062-2.
[37] Bos J, Moes H. Frictional heating of tribological contacts. J Tribol 1995. https://doi.org/10.1115/1.2830596.
[38] Habchi W, Vergne P, Bair S, Andersson O, Eyheramendy D, Morales-Espejel GE. Influence of pressure and temperature dependence of thermal properties of a lubricant on the behaviour of circular TEHD contacts. Tribology Int 2010. https://doi.org/10.1016/j.triboint.2009.10.002.
[39] Reddyhoff T, Schmidt A, Spikes H. Thermal conductivity and flash temperature. Tribology Lett 2019. https://doi.org/10.1007/s11249-018-1133-8.

[40] Habchi W, Bair S. The role of the thermal conductivity of steel in quantitative elastohydrodynamic friction. Tribology Int 2020. https://doi.org/10.1016/j.triboint.2019.105970.
[41] Bair S. High Pressure Rheology for Quantitative Elastohydrodynamics. Elsevier; 2019. https://doi.org/10.1016/c2017-0-03927-7.
[42] Verbelen F, Derammelaere S, Sergeant P, Stockman K. A comparison of the full and half toroidal continuously variable transmissions in terms of dynamics of ratio variation and efficiency. Mech Mach Theory 2018. https://doi.org/10.1016/j.mechmachtheory.2017.10.026.